



# Source-Resolved Variability of Fine Particulate Matter and Human Exposure in an Urban Area

Pablo Garcia Rivera<sup>1</sup>, Brian T. Dinkelacker<sup>1</sup>, Ioannis Kioutsioukis<sup>2</sup>,  
Peter J. Adams<sup>3,4</sup>, and Spyros N. Pandis<sup>5,6</sup>

<sup>1</sup>Department of Chemical Engineering, Carnegie Mellon University, Pittsburgh, PA, 15213

<sup>2</sup>Department of Physics, University of Patras, 26500, Patras, Greece

<sup>3</sup>Department of Civil and Environmental Engineering, Carnegie Mellon University, Pittsburgh, PA, 15213

<sup>4</sup>Department of Engineering and Public Policy, Carnegie Mellon University, Pittsburgh, PA, 15213

<sup>5</sup>Institute of Chemical Engineering Sciences (FORTH/ICE-HT), 26504, Patras, Greece

<sup>6</sup>Department of Chemical Engineering, University of Patras, 26500, Patras, Greece

## Abstract

Increasing the resolution of chemical transport model (CTM) predictions in urban areas is important to capture sharp spatial gradients in atmospheric pollutant concentrations and better inform air quality and emissions controls policies that protect public health. The chemical transport model PMCAMx was used to assess the impact of increasing model resolution on the ability to predict the source-resolved variability and population exposure to PM<sub>2.5</sub> at 36 x 36, 12 x 12, 4 x 4, and 1 x 1 km resolutions over the city of Pittsburgh during typical winter and summer periods (February and July 2017). At the coarse resolution, county-level differences can be observed, while increasing the resolution to 12 x 12 km resolves the urban-rural gradient. Increasing resolution to 4 x 4 km resolves large stationary sources such as power plants and the 1 x 1 km resolution reveals intra-urban variations and individual roadways within the simulation domain. Regional pollutants that exhibit low spatial variability such as PM<sub>2.5</sub> nitrate show modest changes when increasing the resolution beyond 12 x 12 km. Predominantly local pollutants such as elemental carbon



and organic aerosol have gradients that can only be resolved at the 1 x 1 km scale. Contributions from some local sources are enhanced by weighting the average contribution from each source by the population in each grid cell. The average population weighted  $PM_{2.5}$  concentration does not change significantly with resolution, suggesting that extremely high resolution  $PM_{2.5}$  predictions may not be necessary for effective urban epidemiological analysis.

## 1. Introduction

Particulate matter with aerodynamic diameter less than  $2.5\ \mu\text{m}$  ( $PM_{2.5}$ ) contributes to poor air quality throughout large parts of the United States. These particles directly affect visibility (Seinfeld and Pandis, 2006) and have been associated with long and short-term health effects such as premature death due to cardiovascular disease, increased chance of heart attacks and strokes, reduced lung development and function in children and people with lung diseases such as asthma and increases in hospital admissions due to heart and lung disease (Dockery and Pope, 1994).

At high resolutions, emissions from local sources such as commercial cooking, on-road traffic, residential wood combustion, and industrial activities can have sharp gradients that influence the geographical distribution of  $PM_{2.5}$  concentrations. High-resolution measurements of  $PM_1$  have found gradients of up to  $\sim 2\ \mu\text{g m}^{-3}$  between urban background sites and those with high local emissions (Gu et al., 2018; Robinson et al., 2018).

A key limiting factor on the modeling of particulate matter at high resolutions is the geographical distribution of emissions. Previous studies have found that coarse grid emissions interpolated to higher resolutions lead to small to modest improvements in model predictive ability for ozone (Kumar and Russell, 1996; Arunachalam et al., 2006), secondary organic aerosol (Stroud et al., 2011; Fountoukis et al., 2013) and nitrate (Zakoura and Pandis, 2018; Zakoura and Pandis, 2019). Pan et al., (2017) used the default approach from the U.S. Environmental Protection Agency (EPA) National Emissions Inventory (NEI) to allocate county-based emissions to model grid cells at 4 x 4 and 1 x 1 km and found only small changes to model performance for  $\text{NO}_x$  and  $\text{O}_3$ , while the 1 x 1 km case showed more detailed features of emissions and concentrations in heavily polluted areas.



62           Improvements in the resolution of emission inventories have been focused on traffic  
63 as this source exhibits significant variability at high resolutions. Recent approaches to  
64 building high-resolution traffic inventories include origin-destination by vehicle class (Ma  
65 et al., 2020), synthetic population mobility (Elessa Etuman and Coll, 2018) and fuel sales  
66 combined with traffic counts (McDonald and McBride, 2014). Other sectors such as  
67 biomass burning for residential heating and commercial cooking have been identified as  
68 very uncertain in current inventories (Day et al., 2019). Recent versions of the NEI have  
69 made progress addressing the total emissions and temporal distributions of biomass  
70 burning and commercial cooking (Eyth and Vukovich, 2016), but there is still significant  
71 uncertainty on their geographical location at a sub-county scale. Robinson et al. (2018)  
72 found greatly elevated organic aerosol concentrations in the vicinity of numerous  
73 individual restaurants and commercial districts containing groups of restaurants indicating  
74 that commercial cooking is a source of large gradients on the urban scale.

75           Population density and socio-economic indicators of that population, such as  
76 income or access to healthcare, show large gradients in the urban scale. It is important to  
77 assess the exposure of different sub-populations to air pollutants and the resulting health  
78 effects, a concept known as Environmental Justice (Anand, 2002).

79           We use the Particulate Matter Comprehensive Air quality Model with Extensions  
80 (PMCAMx) to study the impact of increasing model resolution on the model's ability to  
81 predict the variability, sources and population exposure of  $PM_{2.5}$  concentrations on the  
82 urban scale in Pittsburgh. We compare predicted variability at 36 x 36, 12 x 12, 4 x 4 and  
83 1 x 1 km resolutions over the city of Pittsburgh during one typical summer and one typical  
84 winter month of 2017. Additional sensitivity simulations were performed to determine  
85 contributions from selected sources to concentrations. The results of the simulations are  
86 used to estimate exposure to  $PM_{2.5}$  at all resolutions and from the selected sources. A  
87 detailed evaluation of the PMCAMx predictions against measurements will be the topic of  
88 a future publication. Overall the model performance was similar to those in previous model  
89 applications in the Eastern US (Fountoukis et al., 2013).

90



## 2. PMCAMx Description

The Particulate Matter Comprehensive Air quality Model with Extensions (PMCAMx) (Tsimpidi et al., 2009; Karydis et al., 2010; Murphy and Pandis, 2010), uses the framework of the CAMx model (Environ, 2006) to describe horizontal and vertical advection and diffusion, emissions, wet and dry deposition, gas, aqueous and aerosol-phase chemistry. A 10-size section aerosol sectional approach is used to dynamically track the evolution of the aerosol mass distribution. The aerosol species modeled include sulfate, nitrate, ammonium, sodium, chloride, elemental carbon, water, primary and secondary organics, and other non-volatile aerosol components. The SAPRC (Statewide Air Pollution Research Center) photochemical mechanism (Carter, 1999) is used for the simulation of gas-phase chemistry. The version of SAPRC used here includes 237 reactions and 91 individual and surrogate species. For inorganic growth, a bulk equilibrium approach was used, assuming equilibrium between the bulk inorganic aerosol and gas phases (Pandis et al., 1993). The partition of the various semivolatile inorganic aerosol components and aerosol water is determined using the ISORROPIA aerosol thermodynamics model (Nenes et al., 1998). The primary and secondary organic aerosol components are described using the volatility basis set approach (Donahue et al., 2006). For primary organic aerosol (POA) ten volatility bins, with effective saturation concentrations ranging from  $10^{-3}$  to  $10^6 \mu\text{g m}^{-3}$  at 298 K are used. Anthropogenic (aSOA) and biogenic (aSOA) are modeled with 4 volatility bins ( $1, 10, 10^2, 10^3 \mu\text{g m}^{-3}$ ) (Murphy and Pandis, 2009) using  $\text{NO}_x$  dependent yields (Lane et al., 2008). More detailed descriptions of PMCAMx can be found in Fountoukis et al. (2011) and Zakoura and Pandis (2018).

## 3. Model Application

PMCAMx was used to simulate air quality over the metropolitan area of Pittsburgh during February and July 2017. For the base-case simulation we used a one-way nested structure with a  $36 \times 36$  km master grid covering the continental United States, with nested grids of  $12 \times 12$  km,  $4 \times 4$  km in South Western Pennsylvania and a  $1 \times 1$  km grid covering the city of Pittsburgh, most of Allegheny County and the upper Ohio River valley (Figure 1a). The  $1 \times 1$  km grid covers a  $72 \times 72$  km area (Figure 1b).



121 The surface concentrations at the boundaries of the 36 x 36 km grid are shown in  
122 Table S1 in the Supplementary Information. These values were applied to all upper air  
123 layers assuming a constant mixing ratio. Horizontal wind components, vertical diffusivity,  
124 temperature, pressure, water vapor, clouds, and rainfall were generated using the Weather  
125 Research and Forecasting (WRF v3.6.1) model over the whole modeling domain with  
126 horizontal resolution of 12 km. The data was interpolated to higher resolutions when  
127 needed. Initial and boundary meteorological conditions for the WRF simulations were  
128 generated from the ERA-Interim global climate re-analysis database, together with the  
129 terrestrial data sets for terrain height, land-use, soil categories, etc. from the United States  
130 Geological Survey (USGS) database. The WRF modeling system was prepared and  
131 configured in a similar way as described by Gilliam and Pleim (2010). This configuration  
132 is recommended for air quality simulations (Hogrefe et al., 2015; Rogers et al., 2013).

133 Emissions were calculated using the EPA's Emission Modeling Platform (v6.3) for  
134 the National Emissions Inventory for 2011 (NEI11) (Eyth and Vukovich, 2016) using the  
135 default 2017 projected values. Base emissions were calculated first at a 12 km resolution  
136 for the full modeling domain using the Sparse Matrix Operator Kernel Emissions  
137 (SMOKE) model and our WRF meteorological data. For the higher resolution grids, the  
138 spatial surrogates provided with Platform v6.3 were used for all sectors except commercial  
139 cooking and on-road traffic for which custom surrogates were developed. The emissions  
140 by all sources together with the chemical composition are summarized in Table 1 (for the  
141 winter period) and Table 2 (for the summer period)..

142 In this work, we used normalized restaurant count to distribute the commercial  
143 cooking emissions in space in the 1x1 km inner domain. Geographical information was  
144 collected for all locations labeled as "restaurant" from the freely accessible Google Places  
145 Application Programming Interface (API) for the western Pennsylvania area, eastern Ohio  
146 and northern West Virginia. Using this new spatial surrogate, PM<sub>2.5</sub> emissions from  
147 commercial cooking are enhanced primarily in the Pittsburgh urban core with a maximum  
148 increase of 1200 kg g<sup>-1</sup> km<sup>-2</sup> (Figure 2a).

149 To accurately capture spatial patterns of on-road traffic, we use the output of a link-  
150 level, origin-destination by vehicle class traffic model of Pittsburgh (Ma et al., 2020). This  
151 traffic model simulates traffic counts and speed by hour-of-day using observations from



Pennsylvania Department of Transportation sites throughout Pittsburgh. As expected, emissions in areas with major highways are high (Figure 2b).

## 4. PM<sub>2.5</sub> concentrations and sources during winter

### 4.1 Effect of grid resolution

The results of the simulations with the four resolutions for the winter period are shown in Figure 3 and Figure 4. For the area of interest, the simulations at 36 x 36 km resolves concentration fields at the county scale. The urban-rural gradient is resolved in the 12 x 12 km simulations. Increasing the resolution to 4 x 4 km, large stationary sources such as power plants and large industrial installations are resolved. Finally, the resolution increase to 1 x 1 km resolves the intra-urban variations in Pittsburgh and medium-sized industrial installations.

In the winter period, the predicted maximum PM<sub>2.5</sub> concentration in the inner domain increases from 10.4  $\mu\text{g m}^{-3}$  at 36x36 km, to 11.8  $\mu\text{g m}^{-3}$  at 12x12, to 12.9  $\mu\text{g m}^{-3}$  at 4x4, and finally to 16.4  $\mu\text{g m}^{-3}$  at 1x1 km (Figure 3), a 58% increase. On the other end, the predicted minimum PM<sub>2.5</sub> concentration changes from 8.2  $\mu\text{g m}^{-3}$  at 36 x 36 km to 7  $\mu\text{g m}^{-3}$  at 12 x 12 and remains practically the same at even higher resolutions. This corresponds to the “background” concentration level for the area during the simulation period, so further resolution enhancements do not change this value. The standard deviation of the predicted concentration can be used as a measure of the concentration variability in the area. This standard deviation changes from 0.9  $\mu\text{g m}^{-3}$  at 36x36, to 1.24  $\mu\text{g m}^{-3}$  at 12x12, to 1.45  $\mu\text{g m}^{-3}$  at 4x4 and to 1.35  $\mu\text{g m}^{-3}$  at 1x1 km. These results indicate an increase of the PM<sub>2.5</sub> variability by 50% when one moves from the coarse to the finest resolution. However, most of this change in variability (38% out of the 50%) appears when one moves from 36x36 to 12x12 km.

Elemental carbon is a primary aerosol component with sources that are quite variable in space. In winter, the predicted maximum PM<sub>2.5</sub> EC increased by a factor of 2.9, from 0.6  $\mu\text{g m}^{-3}$  at the 36 x 36 km resolution to 1.6  $\mu\text{g m}^{-3}$  at 1 x 1 km (Figure 3). The predicted maximum EC is, as expected in the Pittsburgh downtown area. On the other hand, the predicted minimum of EC is reduced by only 0.1  $\mu\text{g m}^{-3}$ , from 0.34  $\mu\text{g m}^{-3}$  at 36x36 km to 0.24  $\mu\text{g m}^{-3}$  at resolutions lower or equal than 4x4 km. The standard deviation of the



183 predicted EC almost doubles from  $0.1 \mu\text{g m}^{-3}$  at  $36 \times 36 \text{ km}$  to  $0.18 \mu\text{g m}^{-3}$  at  $1 \times 1 \text{ km}$ .  
184 Approximately 50% of this increase in variability appears in the transition from the coarse  
185 to the intermediate resolution of  $12 \times 12 \text{ km}$ . The fine and the finest resolutions are needed  
186 to resolve the other half of the predicted variability.

187 During this winter period a significant fraction (79%) of the OA in the Pittsburgh  
188 area is primary and therefore the higher resolution results in increases of the predicted  
189 maximum concentrations in space from  $2.8 \mu\text{g m}^{-3}$  at the coarse resolution to  $3.7 \mu\text{g m}^{-3}$  at  
190 the intermediate to  $4.8 \mu\text{g m}^{-3}$  at the finest resolution (Figure 3). This corresponds to an  
191 increase by a factor of 1.7, more than the change for total  $\text{PM}_{2.5}$ , but much less than that  
192 for EC. The predicted maximum is located in downtown Pittsburgh, with additional  
193 hotspots in neighboring counties that are resolved at the fine and finest resolution. The  
194 predicted minimum changes from  $2.1 \mu\text{g m}^{-3}$  at  $36 \times 36$  to  $1.7 \mu\text{g m}^{-3}$  at  $12 \times 12$  with small  
195 reductions at higher resolutions. The variability (standard deviation) of the OA  
196 concentration field of the predicted concentration increases by a factor of approximately  
197 1.6 from  $0.35 \mu\text{g m}^{-3}$  at  $36 \times 36$ , to  $0.51 \mu\text{g m}^{-3}$  at  $12 \times 12 \text{ km}$ . The increase is small at even  
198 higher resolutions with the standard deviation of OA reaching  $0.53 \mu\text{g m}^{-3}$  at  $1 \times 1 \text{ km}$  (an  
199 increase by a factor of 1.7).

200 The predicted fine nitrate levels are relatively high ranging from 1.78 to  $2.24 \mu\text{g}$   
201  $\text{m}^{-3}$  in the coarse-resolution simulation. This is expected in this wintertime period due to  
202 the partitioning of nitric acid and ammonium in the particulate phase. This predicted  
203 concentration range increases to  $1.5\text{--}2.24 \mu\text{g m}^{-3}$  in the finest scale simulation with higher  
204 levels in the northeast of the domain. The standard deviation of the predicted concentration  
205 does not show any significant trend changing from  $0.19 \mu\text{g m}^{-3}$  at  $36 \times 36$  to  $0.15 \mu\text{g m}^{-3}$   
206 at  $1 \times 1 \text{ km}$ .

207 For  $\text{PM}_{2.5}$  ammonium, changes with increasing resolution are modest with the  
208 predicted minimum being reduced from  $1.07 \mu\text{g m}^{-3}$  at  $36 \times 36$  to approximately  $0.95 \mu\text{g}$   
209  $\text{m}^{-3}$  at all other higher resolutions. The predicted maximum stays relatively constant  
210 between  $1.25 \mu\text{g m}^{-3}$  and  $1.27 \mu\text{g m}^{-3}$  at all resolutions. As with nitrate, the standard  
211 deviation does not show any significant trend changing from  $0.08 \mu\text{g m}^{-3}$  at  $36 \times 36$ , to  $0.09$   
212  $\mu\text{g m}^{-3}$  at  $12 \times 12$ , to  $0.07 \mu\text{g m}^{-3}$  at  $4 \times 4$  and  $1 \times 1 \text{ km}$  resolutions.

213



## 4.2 Source Apportionment

We performed zero-out simulations in the 1x1 km Pittsburgh grid to determine the local contributions of eight source categories to the total  $\text{PM}_{2.5}$ . The local sources quantified included: commercial cooking, industrial, biomass burning, on-road traffic, power generation, and miscellaneous area sources. The miscellaneous area sources sector includes a large variety of emission sources that are not classified in any of the sources in Table 2. These include chemical manufacturing, solvent utilization for surface coatings, degreasing and dry cleaning, storage and transport of petroleum products, waste disposal and incineration, and cremation. The emissions from agricultural dust, river barges, off-road equipment, oil-gas activities, and rail were grouped on the “others” source. All emissions (particulate and gas-phase) from each source were set to zero, and the results of the zero-out simulation were subtracted from those of the baseline simulation to estimate the corresponding source contribution. The contribution of long-range transport from outside the inner domain was also estimated by setting all local sources to zero.

Biomass burning is used during the winter for residential heating and recreation. This source contributes a maximum of  $3.31 \mu\text{g m}^{-3}$  in Cranberry, a northern suburb of Pittsburgh located in the neighboring Butler county. In the downtown Pittsburgh area, the contribution from biomass burning accounts for 7% of the  $\text{PM}_{2.5}$ . This source shows the highest variability with a standard deviation of  $0.5 \mu\text{g m}^{-3}$ .

The maximum contribution of  $8.05 \mu\text{g m}^{-3}$  from industry is predicted near a cluster of industrial facilities in the town of Butler, 37 km northwest of Pittsburgh. The maximum  $\text{PM}_{2.5}$  concentration of the modeling domain is located here. In this location long-range transport contributes 37% of the  $\text{PM}_{2.5}$  followed by industrial sources with 49% and biomass burning with 7%. On average, the contribution from industrial sources is low with 3.7%. In downtown Pittsburgh, the contribution is lower still with 2%.

On-road traffic emissions are most important in major highway intersections and river crossings surrounding downtown Pittsburgh with a maximum contribution of  $3.9 \mu\text{g m}^{-3}$  accounting for 24% of the  $\text{PM}_{2.5}$  in this area. On average, on-road traffic contributes 2.5% of the  $\text{PM}_{2.5}$  mass. The contribution from on-road traffic shows higher variability (standard deviation:  $0.36 \mu\text{g m}^{-3}$ ) since this sector contributes significantly to areas adjacent to the network of highways that radiates from the Pittsburgh downtown.





245 On average, commercial cooking emissions contribute 0.7% of the  $\text{PM}_{2.5}$  in the  
246 modeling domain with a maximum contribution of  $2.44 \mu\text{g m}^{-3}$  in downtown Pittsburgh,  
247 with smaller contributions in the surrounding urban area. Cooking is predicted to account  
248 for 16% of the  $\text{PM}_{2.5}$  mass in downtown Pittsburgh. The contribution from commercial  
249 cooking is localized around downtown Pittsburgh and therefore shows little variability  
250 throughout the domain with a standard deviation of  $0.1 \mu\text{g m}^{-3}$ .

251 The miscellaneous area source sector contributes 6% of the  $\text{PM}_{2.5}$  on average. Since  
252 this sector encompasses a variety of sources and activities, its contribution shows  
253 significant variability with a standard deviation of  $0.34 \mu\text{g m}^{-3}$ . The maximum contribution  
254 is located in the Pittsburgh urban core with  $1.64 \mu\text{g m}^{-3}$ , accounting for 11% of the  $\text{PM}_{2.5}$ .

255 The power generation sector contributes a maximum of  $0.63 \mu\text{g m}^{-3}$  in the plume  
256 of the Bruce Mansfield power plant northwest of Pittsburgh. This sector shows the smallest  
257 variability with  $0.09 \mu\text{g m}^{-3}$ .

258 Long-range transport from outside the inner modeling domain is the major source  
259 of  $\text{PM}_{2.5}$  during this period contributing an average of 74%. This contribution varies from  
260  $7.1 \mu\text{g m}^{-3}$  in the southeast corner of the domain decreasing in the direction of the Pittsburgh  
261 urban core where the contribution is reduced to  $5.9 \mu\text{g m}^{-3}$ . In areas where there are  
262 significant local emissions such as the Pittsburgh downtown, the contribution from long-  
263 range transport decreases to 38%.

264 Contributions for all remaining sources are largest in the Pittsburgh downtown with  
265  $0.74 \mu\text{g m}^{-3}$ , accounting for 5% of the  $\text{PM}_{2.5}$ . This sector also significantly contributes on  
266 the Ohio and Monongahela river valleys, where there is important rail and river traffic. On  
267 average, these sources contribute 3% of the  $\text{PM}_{2.5}$  and show a moderate variability with a  
268 standard deviation of  $0.1 \mu\text{g m}^{-3}$ .

269 For all local sources, the minimum contribution is close to zero (less than  $0.1 \mu\text{g m}^{-3}$ )  
270 and is located at the southwestern corner of the domain, near the Ohio – West Virginia  
271 border.

272



## 5. PM<sub>2.5</sub> concentrations and sources during summer

### 5.1 Effect of grid resolution

The predicted PM<sub>2.5</sub> concentrations in the simulated summer period are lower than during the winter period and more uniform, however, the qualitative behavior of the model at the different scales remains the same (Figure 6). The standard deviation of the PM<sub>2.5</sub> increases from 0.28  $\mu\text{g m}^{-3}$  at 36 x 36, to 0.57  $\mu\text{g m}^{-3}$  at 12 x 12, to 0.72  $\mu\text{g m}^{-3}$  at 4 x 4 and to 0.82  $\mu\text{g m}^{-3}$  at 1 x 1 km. At the finest scale, the predicted variability in the summer is 61% of that in the winter. Similar to the winter period, the predicted maximum PM<sub>2.5</sub> concentration changes significantly with increasing resolution. The predicted maximum PM<sub>2.5</sub> increases from 6.4  $\mu\text{g m}^{-3}$  at the coarse to 15.3  $\mu\text{g m}^{-3}$  at the fine resolution. The finest scale better resolves the concentration field in the cluster of industrial installations 37 km northwest of Pittsburgh. The minimum PM<sub>2.5</sub> drops from 6.5  $\mu\text{g m}^{-3}$  at 36 x 36 to 5.3  $\mu\text{g m}^{-3}$  at 12 x 12, and then to 4.7  $\mu\text{g m}^{-3}$  at 1 x 1 km. As in the winter period, the moderate resolution appears to capture the majority of the concentration change from increasing resolution (67%).

The average EC is lower during the summer with 0.28  $\mu\text{g m}^{-3}$  versus 0.43  $\mu\text{g m}^{-3}$  in the winter. The standard deviation of the predicted average EC increases from 0.06  $\mu\text{g m}^{-3}$  at 36 x 36, to 0.09  $\mu\text{g m}^{-3}$  at 12 x 12, to 0.11  $\mu\text{g m}^{-3}$  at 4 x 4 km, and to 0.13  $\mu\text{g m}^{-3}$  at 1 x 1 km. The peak average EC is located in downtown Pittsburgh and increases by a factor of 3.6 (from 0.35 to 1.27  $\mu\text{g m}^{-3}$ ) moving from the coarse to the finest resolution. It is noteworthy that the peak is 38% less than that of the winter when the coarse resolution is used, but only 21% when the finest resolution is used. The concentration range (difference between the maximum and the minimum) increases from 0.13  $\mu\text{g m}^{-3}$  to 1.12  $\mu\text{g m}^{-3}$  moving from the coarse to the finest resolution. This increase by a factor of 8.6 shows the importance of the local variations of a primary species like EC in an urban area in both summer and winter.

The OA concentration field is quite uniform at the coarse-scale varying by only 0.17  $\mu\text{g m}^{-3}$  (from 1.72 to 1.89  $\mu\text{g m}^{-3}$ ) with a standard deviation of 0.07  $\mu\text{g m}^{-3}$  (Figure 6). Variability increases significantly when one moves to the finest scale, with the range increasing to 2.24  $\mu\text{g m}^{-3}$  (from 1.55 to 3.79  $\mu\text{g m}^{-3}$ ) and the standard deviation of the OA



field increases to  $0.2 \mu\text{g m}^{-3}$ . The use of the finest scale appears to be needed for the resolution of the OA high concentration areas in the summer more than in the winter.

The  $\text{PM}_{2.5}$  sulfate levels during the summer period are on average 12% higher during the summertime period. At the coarse and intermediate scales, the predicted average concentration fields have relatively little structure (Figure 7). The corresponding concentration ranges are relatively narrow ( $0.05 \mu\text{g m}^{-3}$  at  $36 \times 36 \text{ km}$  and  $0.42 \mu\text{g m}^{-3}$  at  $12 \times 12 \text{ km}$ ). However, a different picture emerges at the fine and especially the finest scales. The plumes from the major power plants can be clearly seen at these higher resolutions. The maximum increased by  $0.5 \mu\text{g m}^{-3}$  from the coarse scale to the finest scale while the minimum is reduced from  $1.78 \mu\text{g m}^{-3}$  at  $36 \times 36$  to  $1.05 \mu\text{g m}^{-3}$  at  $12 \times 12$ , to  $0.95 \mu\text{g m}^{-3}$  at  $4 \times 4$  and  $1 \times 1 \text{ km}$ . The standard deviation of the predicted sulfate concentration field at the coarse resolution is low and similar to that in winter,  $0.02 \mu\text{g m}^{-3}$ . However, the variability at the finest scale in the summer ( $0.13 \mu\text{g m}^{-3}$  at  $1 \times 1 \text{ km}$ ) is twice the predicted variability in the winter.

The predicted summertime nitrate concentrations are quite low in the area (average  $0.5 \mu\text{g m}^{-3}$  in the coarse and  $0.46 \mu\text{g m}^{-3}$  in the finest resolution). The predicted minimum decreases from  $0.42 \mu\text{g m}^{-3}$  at  $36 \times 36$  to  $0.39 \mu\text{g m}^{-3}$  at  $12 \times 12$ , to  $0.34 \mu\text{g m}^{-3}$  at  $4 \times 4$ , and to  $0.3 \mu\text{g m}^{-3}$  at  $1 \times 1 \text{ km}$ . The predicted maximum concentration increases from  $0.56 \mu\text{g m}^{-3}$  at the coarse scale to  $0.71 \mu\text{g m}^{-3}$  at the intermediate scale and stays relatively constant at higher resolutions. The concentration field is quite uniform with a standard deviation ranging from  $0.06$  to  $0.09 \mu\text{g m}^{-3}$  for all scales. However, due to the reduction in the predicted minimum the concentration range increases from  $0.14 \mu\text{g m}^{-3}$  at the coarse resolution to  $0.37 \mu\text{g m}^{-3}$  at the finest resolution.

The  $\text{PM}_{2.5}$  ammonium concentration field is quite uniform at all resolutions (Figure 7). The concentration range increases from  $0.04$  to  $0.22 \mu\text{g m}^{-3}$  moving from the coarse to the finest resolution and the standard deviation increases from  $0.02$  to  $0.04 \mu\text{g m}^{-3}$ .

## 5.2 Source Apportionment

During summer, residential biomass burning is minimal. This source contributes a maximum of  $0.04 \mu\text{g m}^{-3}$  and an average of  $0.007 \mu\text{g m}^{-3}$ , accounting for 0.6% of the average total  $\text{PM}_{2.5}$ .



334 Power generation sources have the highest average contribution to total  $\text{PM}_{2.5}$  of  
335 all the local sources of 10%. Industrial sources account for 6% of the average  $\text{PM}_{2.5}$  but are  
336 the most important contributor in the point of the modeling domain with the maximum  
337 predicted  $\text{PM}_{2.5}$  concentration. At this location in Butler County, industrial sources account  
338 for 58% of total  $\text{PM}_{2.5}$

339 As in the winter period, on-road traffic emissions have the largest contribution to  
340 the  $\text{PM}_{2.5}$  in the downtown Pittsburgh area where four large highways intersect. In this  
341 location on-road traffic contributes 26% of the  $\text{PM}_{2.5}$ . On average, local on-road traffic  
342 contributes around 3% of the  $\text{PM}_{2.5}$  mass. During the summer period, the variability of the  
343 on-road traffic contribution is slightly lower with  $0.33 \mu\text{g m}^{-3}$  compared with  $0.36 \mu\text{g m}^{-3}$   
344 during winter.

345 Commercial cooking emissions contribute a maximum of  $2.08 \mu\text{g m}^{-3}$  to the  
346 average total  $\text{PM}_{2.5}$  in downtown Pittsburgh. This source accounts for 17% of the  $\text{PM}_{2.5}$  in  
347 the city but only 1% for the entire modeling domain.

348 On average, the miscellaneous area sources sector contributes  $0.26 \mu\text{g m}^{-3}$   
349 accounting for 4.3% of the  $\text{PM}_{2.5}$ . In downtown Pittsburgh, where the contribution is  
350 highest, this source contributes 7% of the  $\text{PM}_{2.5}$ .

351 Unlike in the winter period, the plumes from major powerplants in the Ohio river  
352 valley are clearly resolved in the summer. The power generation sector contributes a  
353 maximum of  $2.4 \mu\text{g m}^{-3}$  in the plume of the Bruce Mansfield power plant northwest of  
354 Pittsburgh. On average, the 9.4% contribution from this sector to the  $\text{PM}_{2.5}$  is much larger  
355 than in the winter where it only contributed 2.3%. The plume from the Mitchell power  
356 plant in the southwest corner of the modeling domain is clearly resolved and reaches all  
357 the way to the city. This increases the contribution from power generation to the  $\text{PM}_{2.5}$  in  
358 the downtown core from  $0.22 \mu\text{g m}^{-3}$  in the winter to  $0.61 \mu\text{g m}^{-3}$  in the summer. The  
359 maximum contribution of  $8.98 \mu\text{g m}^{-3}$  from industrial sources is a cluster of industrial  
360 facilities in the town of Butler, northwest of Pittsburgh.

361 Long-range transport from sources outside the region contributes a maximum of  
362  $5.2 \mu\text{g m}^{-3}$  in the southeast corner of the domain decreasing in the direction of the Pittsburgh  
363 northern suburbs where the contribution is minimal with  $4.1 \mu\text{g m}^{-3}$ . On average, long-



range transport accounts for 72% of the  $\text{PM}_{2.5}$  mass. In downtown Pittsburgh, long-range transport contributes  $4.24 \mu\text{g m}^{-3}$  accounting for 35% of the  $\text{PM}_{2.5}$ .

On average, the contribution from all remaining sources is 3.6% and shows a moderate variability of  $0.10 \mu\text{g m}^{-3}$ . The contribution from these sources is maximal in downtown Pittsburgh with  $0.78 \mu\text{g m}^{-3}$  accounting for 6% of the  $\text{PM}_{2.5}$ .

For all local sources, the minimum contribution is close to zero (less than  $0.1 \mu\text{g m}^{-3}$ ) and is located at the northwestern corner of the domain, near the Ohio – Pennsylvania border.

Relative contributions of all local sources to domain average predicted total  $\text{PM}_{2.5}$  are shown in Figure 9. The largest differences between February and July are the contributions from biomass burning and power generation. In the winter, biomass burning is the most important local source of  $\text{PM}_{2.5}$ , contributing over 8%. In the summer, this source contributes much less than 1% to total  $\text{PM}_{2.5}$ . This discrepancy can easily be explained by the lack of residential wood combustion in the warmer months of the year. Power generation is a significantly more important source in July than in February. This is likely a result of a lower mixing height in the winter combined with emissions plumes from power plants in the Ohio river valley originating from very tall stacks.

The relative contributions of local sources to average predicted total  $\text{PM}_{2.5}$  in the maximum concentration cell in Butler County and in downtown Pittsburgh are shown in Figures 10 and 11, respectively. The dominant local source in the Butler County location is industrial emissions, due to the proximity of various industrial installations in this area. Industrial sources here account for around 49% of total  $\text{PM}_{2.5}$  in February and 58% of total  $\text{PM}_{2.5}$  in July. A lot of the difference in industrial  $\text{PM}_{2.5}$  at the Butler County location between months is made up by biomass burning in February, which accounts for 7% more of the total compared to July.

## 6. Exposure to $\text{PM}_{2.5}$

The population data in the inner domain from the 2010 U.S. census was used to estimate the exposure of the population in the Pittsburgh area to model predictions of  $\text{PM}_{2.5}$  during winter of 2017 at the different grid resolutions. We ranked the average  $\text{PM}_{2.5}$  concentrations from all the cells in the modeling domain and created bins of  $0.2 \mu\text{g m}^{-3}$ . A



sum of the population from all the grid cells that fall within each concentration bin was calculated and divided by the total population of the inner grid to construct population exposure histograms.

### 6.1 Winter PM<sub>2.5</sub> Exposure

Figure 12 shows the population exposure histograms for the Pittsburgh area (inner domain) for each model resolution. At the coarse resolution, there are only four PM<sub>2.5</sub> values and 46% of the population is exposed to a concentration of 10.4  $\mu\text{g m}^{-3}$  with decreasing exposure with PM<sub>2.5</sub> concentration. At a 12 km resolution, the low concentration side of the distribution is better resolved but gaps can still be observed at higher levels. At this intermediate resolution, the largest fraction of the population (15%) is exposed to PM<sub>2.5</sub> concentrations of 11.8  $\mu\text{g m}^{-3}$ .

When the resolution is increased to 4 km the biggest improvements on the model ability to resolve the exposure distribution happen at concentrations higher than 9.4  $\mu\text{g m}^{-3}$ . At the fine resolution, no gaps appear in the distribution. A maximum of 12% of the population is exposed to PM<sub>2.5</sub> concentrations of 12  $\mu\text{g m}^{-3}$  while at the highest concentration of 12.8  $\mu\text{g m}^{-3}$  3% are exposed. At the 1 km resolution, the distribution is much smoother due to the ability of this finest grid to capture local gradients. The largest fraction of the population (6%) is exposed to PM<sub>2.5</sub> concentrations of 9.2  $\mu\text{g m}^{-3}$ . At the highest concentration of 14.4  $\mu\text{g m}^{-3}$  the exposed population is less than 0.1% as this maximum point is located near industrial installations 37 km northwest of Pittsburgh where the population density is very low.

At resolutions of 36 km, 12 km, 4 km, and 1 km the predicted average population weighted total PM<sub>2.5</sub> concentration during February 2017 is 9.74  $\mu\text{g m}^{-3}$ , 9.77  $\mu\text{g m}^{-3}$ , 10.28  $\mu\text{g m}^{-3}$ , and 10.00  $\mu\text{g m}^{-3}$ , respectively. This represents an increase of only 2.6% when moving from lowest to highest resolution. Relative contributions of local sources to average population weighted PM<sub>2.5</sub> concentration is shown in Figure 14. Compared to the domain average PM<sub>2.5</sub> concentrations (Figure 9), many local source contributions are enhanced in terms of average population exposure. In February, weighting PM<sub>2.5</sub> concentrations by population increases the contribution from biomass burning from 8.3% to 11.7%. Other notable increases include onroad traffic (2.5% to 6.5%), and miscellaneous



area sources (5.9% to 9.2%). Other local source contributions to population weighted  $\text{PM}_{2.5}$  were similar to the corresponding non-weighted concentrations.

## 6.2 Summer $\text{PM}_{2.5}$ Exposure

Figure 14 shows the population exposure for each simulation grid during the summer period. At the coarse resolution, 88% of the population is exposed to a concentration of 7 to  $7.2 \mu\text{g m}^{-3}$ . At 12 x 12 km resolution, the exposure distribution is better resolved but a gap is still present at  $7.2 \mu\text{g m}^{-3}$  and exposure to  $\text{PM}_{2.5}$  concentrations above  $7.6 \mu\text{g m}^{-3}$  is not resolved at all. At this intermediate resolution, the largest fraction of the population (19%) is exposed to  $\text{PM}_{2.5}$  concentrations of  $7.4 \mu\text{g m}^{-3}$ . Increasing the resolution to 4 x 4 km both shifts the distribution to slightly lower concentrations and resolves exposure to higher  $\text{PM}_{2.5}$  concentrations than with the 12 x 12 km grid. At this resolution, 14% of the population is exposed to  $6.4 \mu\text{g m}^{-3}$  and smaller portions of the population are exposed to concentrations higher than  $8.0 \mu\text{g m}^{-3}$ . Moving to the highest resolution grid further resolves the exposure distribution. Most notably, 1 x 1 km resolution reveals a bimodal distribution of population exposure, with one peak centered around  $6.0 \mu\text{g m}^{-3}$  and another centered around  $7.4 \mu\text{g m}^{-3}$ . This likely corresponds to one subset of the population in the urban areas of Pittsburgh who are exposed to higher  $\text{PM}_{2.5}$  concentrations and another subset representing the surrounding suburban areas.

At resolutions of 36 km, 12 km, 4 km, and 1 km the predicted average population weighted total  $\text{PM}_{2.5}$  concentration during February 2017 is  $7.06 \mu\text{g m}^{-3}$ ,  $6.78 \mu\text{g m}^{-3}$ ,  $7.00 \mu\text{g m}^{-3}$ , and  $6.99 \mu\text{g m}^{-3}$ , respectively. This represents just a 1% decrease between the lowest and highest resolutions. Similar to the effect seen in February, weighting  $\text{PM}_{2.5}$  concentrations by population increases the contribution from onroad traffic from 3.3% to 8.9% in July. Contributions from miscellaneous area sources also increased (4.3% to 7.1%) when weighting by population. The population weighted contribution from power generation sources in July decreased from the non-weighted value from 9.4% to 8.3%. All other local source contributions to population weighted  $\text{PM}_{2.5}$  in July were similar to the non-weighted values.



## 7. Conclusions

We applied the PMCAMx chemical transport model over the city of Pittsburgh for the simulation periods of February and July 2017 using a series of telescoping grids at 36 x 36 km, 12 x 12 km, 4 x 4 km and 1 x 1 km. Emissions were calculated using 2017 projections from the 2011 NEI. Emissions were distributed geographically using the spatial surrogates provided with the NEI11 for all grids. For commercial cooking, a new 1 x 1 km spatial surrogate was developed using restaurant count data from the Google Places API. Traffic model data was used to develop a 1 x 1 km spatial surrogate for on-road traffic emissions.

At the coarse resolution, county-level differences can be observed. Increasing the resolution to 12 x 12 km resolves the urban-rural gradient and further increasing to 4 x 4 resolves large stationary sources such as power plants. Only at the finest resolution intra-urban variations and individual roadways are resolved. Low variability, regional pollutants such as nitrate show limited improvement after increasing the resolution to 12 x 12 km while predominantly local pollutants such as elemental carbon and winter organic aerosol have gradients that can only be resolved at the finest resolution.

Biomass burning shows the largest variability during the winter period with many local maxima and significant emissions within the city and in the suburbs. During the summer contributions from this source are negligible. In contrast with the winter period, during the summer the plumes from large power plants in the Ohio river valley can be resolved. These plumes are rich in sulfates and start being resolved at 4 x 4 km with significant detail added at 1 x 1 km. During both periods the largest contributing source to the average PM<sub>2.5</sub> is particles from outside the modeling domain.

The ability of the model to resolve the exposure distribution increases at different rates according to the concentration. A significant improvement in resolving exposure to concentrations below 9.4  $\mu\text{g m}^{-3}$  in the winter and below 7.0  $\mu\text{g m}^{-3}$  in the summer is achieved by increasing the resolution to 12 x 12 km. Only at the finest resolution is the exposure to concentrations above 9.6  $\mu\text{g m}^{-3}$  in the winter and above 8.6  $\mu\text{g m}^{-3}$  in the summer fully resolved as well as the impact of high concentration spots.

The average exposure in terms of average contribution to population weighted PM<sub>2.5</sub> concentrations of some local sources is enhanced compared to the non-weighted





487 average  $\text{PM}_{2.5}$  concentrations. In February, weighting by population enhanced the  
488 contributions from biomass burning, onroad traffic, and miscellaneous area sources by 3-  
489 4%. In July, the contributions from onroad traffic and miscellaneous area sources also  
490 increased by 3-5% from this procedure.

491 It was determined that increasing simulation grid resolution from 36 x 36 km to 1  
492 x 1 km had minimal effect on the predicted domain average population weighted  $\text{PM}_{2.5}$   
493 concentration. Moving from the lowest to highest grid resolution increased the predicted  
494 average population weighted  $\text{PM}_{2.5}$  by less than 3%. In July, the average decreased by 1%.  
495 This negligible change in the predicted average exposure to  $\text{PM}_{2.5}$  suggests that extremely  
496 high resolution predictions of urban  $\text{PM}_{2.5}$  pollution may not be necessary for accurate  
497 epidemiological analysis, however the increased neighborhood scale resolution could be  
498 vital for topics related to environmental justice

499

## 500 **8. Code and data availability**

501 The code and simulation results are available upon request  
502 (spyros@chemeng.upatras.gr).

503

## 504 **9. Supplement**

505

## 506 **10. Author contributions**

507 P.G.R. and B.T.D. performed the PMCAMx simulations, analyzed the results and  
508 wrote the manuscript. P.G.R. prepared the anthropogenic emissions and other inputs for  
509 the simulations. I.K. set-up the WRF simulations and assisted in the preparation of the  
510 meteorological inputs. S.N.P. and P.J.A. designed and coordinated the study and helped  
511 in the writing of the paper. All authors reviewed and commented on the manuscript.

512

## 513 **11. Competing interests**

514 The authors declare that they have no conflict of interest.

515

516



517 **12. Financial Support**

518           This work was supported by the Center for Air, Climate, and Energy Solutions  
519 (CACES) which was supported under Assistance Agreement No. R835873 awarded by the  
520 U.S. Environmental Protection Agency and the Horizon-2020 Project REMEDIA of the  
521 European Union under grant agreement No 874753.

522

523



### 13. References

- Anand, S.: The concern for equity in health. *Journal of Epidemiology & Community Health* 56, 485–487, 2002.
- Arunachalam, S., Holland, A., Do, B., Abraczinskas, M.: A quantitative assessment of the influence of grid resolution on predictions of future-year air quality in North Carolina, USA. *Atmospheric Environment* 40, 5010–5026, 2006.
- Carter, W. P. L.: Documentation of the SAPRC-99 chemical mechanism for VOC reactivity assessment, 1999.
- Day, M., Pouliot, G., Hunt, S., Baker, K.R., Beardsley, M., Frost, G., Mobley, D., Simon, H., Henderson, B., Yelverton, T., Rao, V.: Reflecting on progress since the 2005 NARSTO emissions inventory report. *Journal of the Air & Waste Management Association* 69, 1025–1050, 2019.
- Dockery, D. W., Pope, C. A.: Acute respiratory effects of particulate air pollution. *Annual Review of Public Health* 15, 107–132, 1994.
- Elessa Etuman, A., Coll, I.: OLYMPUS v1.0: Development of an integrated air pollutant and GHG urban emissions model-methodology and calibration over greater Paris. *Geoscientific Model Development* 11, 5085–5111, 2018.
- Eyth, A., Vukovich, J.: Technical Support Document (TSD): Preparation of Emissions Inventories for the Version 6.2, 2011 Emissions Modeling Platform, 2016.
- Fountoukis, C., Koraj, D., Denier van der Gon, H. A. C., Charalampidis, P. E., Pilinis, C., Pandis, S. N.: Impact of grid resolution on the predicted fine PM by a regional 3-D chemical transport model. *Atmospheric Environment* 68, 24–32, 2013.
- Fountoukis, C., Racherla, P. N., Denier van der Gon, H. A. C., Polymeneas, P., Charalampidis, P. E., Pilinis, C., Wiedensohler, A., Dall'Osto, M., O'Dowd, C., Pandis, S. N.: Evaluation of a three-dimensional chemical transport model (PMCAMx) in the European domain during the EUCAARI May 2008 campaign. *Atmospheric Chemistry and Physics* 11, 10331–10347, 2011.
- Gilliam, R. C., Pleim, J. E.: Performance assessment of new land surface and planetary boundary layer physics in the WRF-ARW. *Journal of Applied Meteorology and Climatology* 49, 760–774, 2010.
- Gu, P., Li, H. Z., Ye, Q., Robinson, E. S., Apte, J. S., Robinson, A. L., Presto, A. A.:



- 555 Intracity variability of particulate matter exposure is driven by carbonaceous sources  
 556 and correlated with land-use variables. *Environmental Science and Technology* 52,  
 557 11545–11554, 2018.
- 558 Hogrefe, C., Pouliot, G., Wong, D., Torian, A., Roselle, S., Pleim, J., Mathur, R.: Annual  
 559 application and evaluation of the online coupled WRF-CMAQ system over North  
 560 America under AQMEII phase 2. *Atmospheric Environment* 115, 683–694, 2015.
- 561 Kumar, N., Russell, A. G.: Multiscale air quality modeling of the Northeastern United  
 562 States. *Atmospheric Environment* 30, 1099–1116, 1996.
- 563 Lane, T. E., Donahue, N. M., Pandis, S. N.: Effect of NO<sub>x</sub> on secondary organic aerosol  
 564 concentrations. *Environmental Science & Technology* 42, 6022–6027, 2008.
- 565 Ma, W., Pi, X., Qian, S.: Estimating multi-class dynamic origin-destination demand  
 566 through a forward-backward algorithm on computational graphs. *Transportation*  
 567 *Research Part C: Emerging Technologies*, 119, 102747, doi:10.1016/j.trc.2020.  
 568 102747, 2020.
- 569 McDonald, B., McBride, Z.: High-resolution mapping of motor vehicle carbon dioxide  
 570 emissions. *Journal of Geophysical Research*, 119, 5283–5298, 2014.
- 571 Pan, S., Choi, Y., Roy, A., Jeon, W.: Allocating emissions to 4 km and 1 km horizontal  
 572 spatial resolutions and its impact on simulated NO<sub>x</sub> and O<sub>3</sub> in Houston, TX.  
 573 *Atmospheric Environment* 164, 398–415, 2017.
- 574 Pandis, S. N., Wexler, A. S., Seinfeld, J. H.: Secondary organic aerosol formation and  
 575 transport - II. Predicting the ambient secondary organic aerosol size distribution.  
 576 *Atmospheric Environment*, 27, 2403–2416, 1993.
- 577 Robinson, E. S., Gu, P., Ye, Q., Li, H. Z., Shah, R. U., Apte, J. S., Robinson, A. L., Presto,  
 578 A. A.: Restaurant impacts on outdoor air quality: Elevated organic aerosol mass from  
 579 restaurant cooking with neighborhood-scale plume extents. *Environmental Science*  
 580 *and Technology* 52, 9285–9294, 2018.
- 581 Rogers, R. E., Deng, A., Stauffer, D. R., Gaudet, B. J., Jia, Y., Soong, S. T., Tanrikulu, S.:  
 582 Application of the weather research and forecasting model for air quality modeling in  
 583 the San Francisco bay area. *Journal of Applied Meteorology and Climatology* 52,  
 584 1953–1973, 2013.
- 585 Seinfeld, J. H., Pandis, S. N.: *Atmospheric Chemistry and Physics: From Air Pollution to*



586        Climate Change, 2nd. ed. John Wiley & Sons, Inc., Hoboken, 2006.

587    Stroud, C. A., Makar, P. A., Moran, M. D., Gong, W., Gong, S., Zhang, J., Hayden, K.,

588        Mihele, C., Brook, J. R., Abbatt, J. P. D., Slowik, J. G.: Impact of model grid spacing

589        on regional- and urban-scale air quality predictions of organic aerosol. *Atmospheric*

590        *Chemistry and Physics* 11, 3107–3118, 2011.

591    Zakoura, M., Pandis, S. N.: Overprediction of aerosol nitrate by chemical transport

592        models: The role of grid resolution. *Atmospheric Environment* 187, 390–400, 2018.

593    Zakoura, M., Pandis, S. N.: Improving fine aerosol nitrate predictions using a Plume-in-

594        Grid modeling approach. *Atmospheric Environment* 116887, doi:10.1016/j.atmosenv.

595        2019.116887, 2019.

596

597



**Table 1.** PM<sub>2.5</sub> emissions by source for the 1 x 1 km Pittsburgh domain (February 2017).

Source Type	Emissions (kg d <sup>-1</sup> km <sup>-2</sup> )								
	PM <sub>2.5</sub>	OA	EC	Chl.	Na	Amm.	Nitrate	Sulfate	Other
Agricultural dust	68.7	9.7	0.4	0.2	0.1	0.1	0.1	0.7	57.2
River barges	19.0	4.2	14.7	0.0	0.0	0.0	0.0	0.1	0.1
Cooking	242	223	8.3	2.2	0.8	0.0	1.1	0.6	6.0
Misc. area sources	683	445	56.7	30.5	3.0	5.6	1.7	42	97.8
Off-road	147	56.2	73.1	0.3	0.1	0.0	0.3	1.1	16.1
Oil-gas (Area)	35.3	1.7	0.0	0.0	0.0	0.0	0.1	8.3	23.2
On-road traffic	188	84.6	75.2	0.3	0.1	1.8	0.6	8.3	16.4
Rail	40.7	8.9	31.4	0.0	0.0	0.0	0.0	0.1	0.2
Biomass burning	1,869	1,696	105	5.6	1.8	2.8	3.6	7.7	46.3
Power generation	3,517	201	194	2.8	0.0	15.7	2.6	460	2,641
Industrial	1,106	192	134	79.4	65.3	10.1	21.1	173	428
Oil-gas (point)	2.8	1.0	1.1	0.0	0.0	0.0	0.1	0.2	0.5

**Table 2.** PM<sub>2.5</sub> emissions by source for the 1 x 1 km Pittsburgh domain (July 2017).

Source Type	Emissions (kg d <sup>-1</sup> km <sup>-2</sup> )								
	PM <sub>2.5</sub>	OA	EC	Chl.	Na	Amm.	Nitrate	Sulfate	Other
Agricultural dust	67.3	8.9	0.4	0.1	0.1	0.1	0.1	0.7	56.9
River barges	19.0	4.2	14.7	0.0	0.0	0.0	0.0	0.1	0.1
Cooking	242	223	8.3	2.2	0.8	0.0	1.1	0.6	6
Misc. area sources	593	392	49.1	28.5	2.5	5.3	1.1	33	81.6
Off-road	205	83.5	92.9	0.2	0.1	0.0	0.4	1.1	27.3
Oil-gas (Area)	35.9	1.9	0.0	0.0	0.0	0.0	0.1	8.9	25.0
On-road traffic	162	67.6	66	0.4	0.1	1.5	0.5	8.6	17.2
Rail	40.7	8.9	31.4	0.0	0.0	0.0	0.0	0.1	0.2
Biomass burning	24.3	22	1.4	0.0	0.0	0.0	0.0	0.1	0.6
Power generation	3,780	216	208	3.1	0.0	16.9	2.8	495	2,840
Industrial	1,050	188	133	67.3	56.2	9.9	21.0	165	412
Oil-gas (point)	2.8	1.0	1.1	0.0	0.0	0.0	0.1	0.2	0.5



**Table S1.** Outer (CONUS) boundary condition concentrations of major aerosol species.

Component	Concentration ( $\mu\text{g m}^{-3}$ )			
	West	East	South	North
Nitrate	0.01	0.01	0.03	0.03
Ammonium	0.14	0.25	0.24	0.16
Sulfate	0.64	1.12	0.81	0.68
Elemental carbon	0.04	0.05	0.09	0.03
Organic aerosol (Winter)	0.20	0.16	0.58	0.80
Organic aerosol (Summer)	0.80	0.80	0.80	0.80

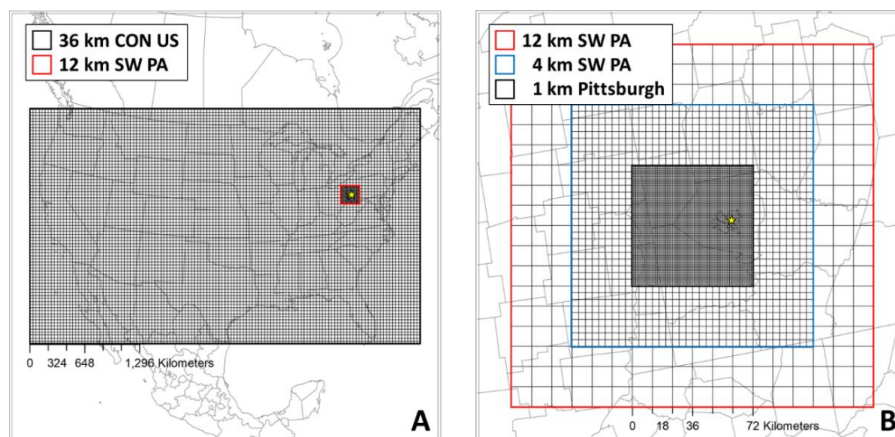


**Figure 1.** Modeling domain used for the PMCAMx simulations. (A) 36 x 36 km continental U.S. grid. (B) 12 x 12 and 4 x 4 km South Western Pennsylvania grids, and 1 x 1 km Pittsburgh nested grids.

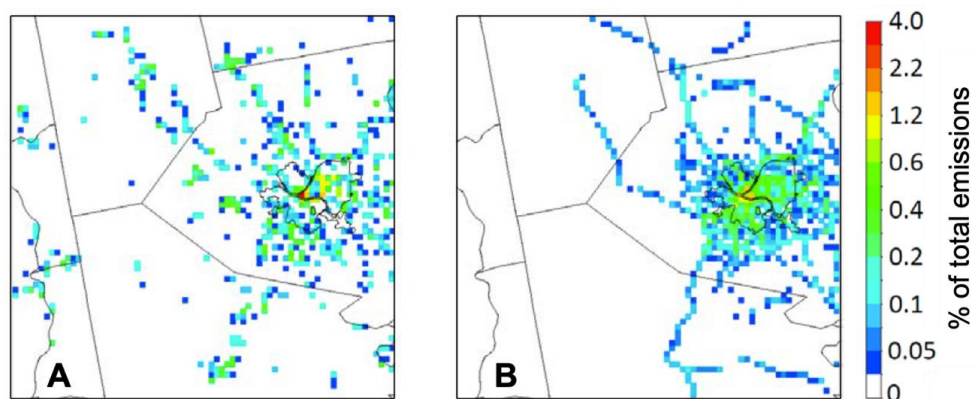


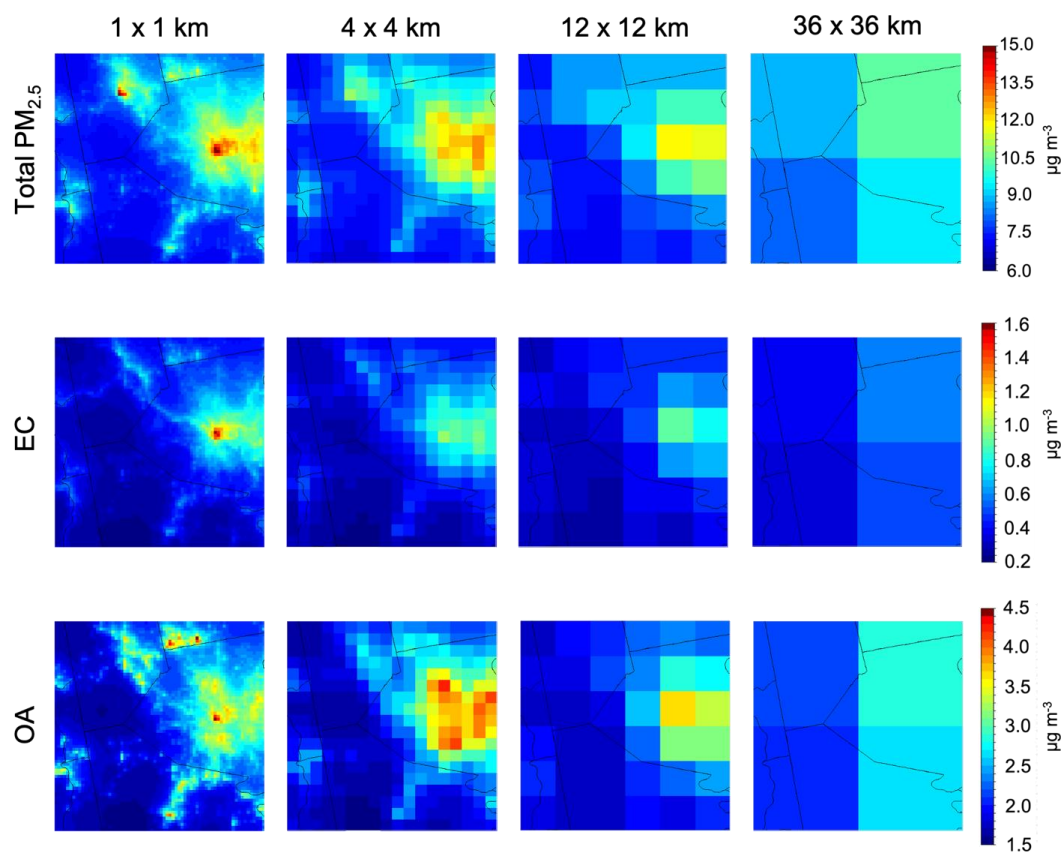
**Figure 2.** Percentage of PM<sub>2.5</sub> emissions in each 1x1 km computational cell for: (A) commercial cooking and (B) on road traffic.





622

623



624

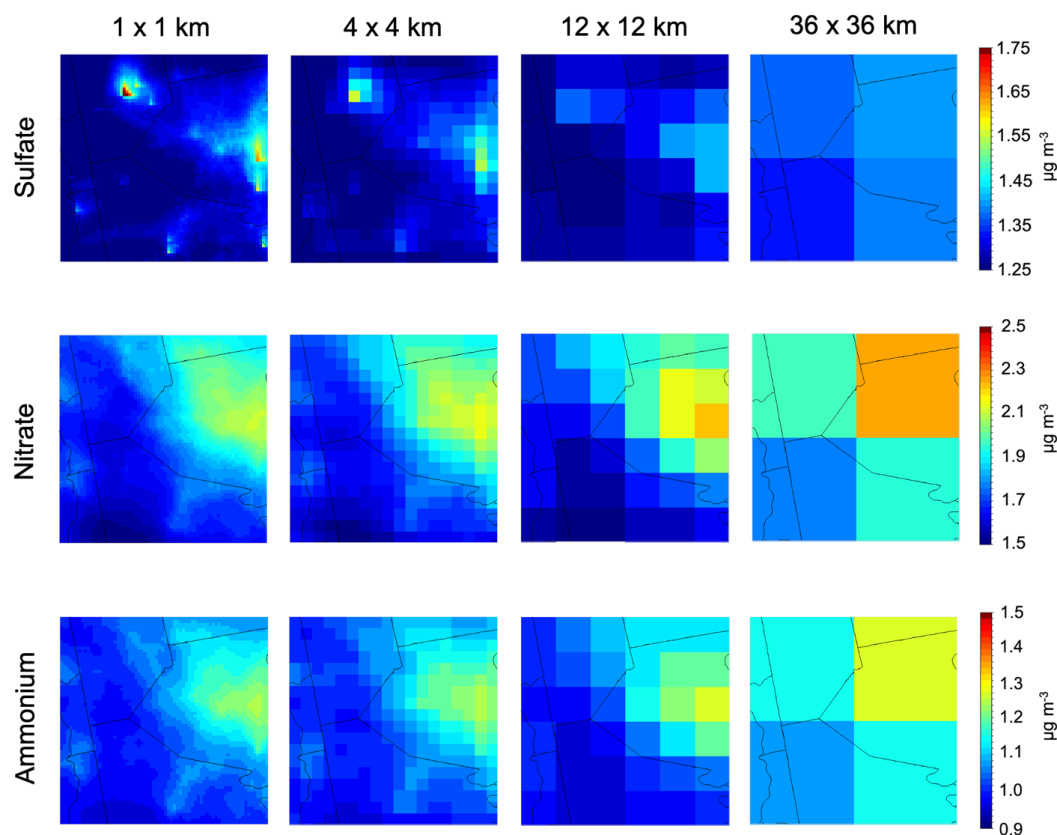
625 **Figure 3** Average predicted ground-level concentration of total PM<sub>2.5</sub>, EC, and OA at 36  
 626 x 36, 12 x 12, 4 x 4 and 1 x 1 km resolutions during February 2017. Different scales are  
 627 used for the various maps.

628



629

630



631

632 **Figure 4.** Average predicted ground-level concentration of PM<sub>2.5</sub> sulfate, nitrate and  
 633 ammonium at a 36 x 36, 12 x 12, 4 x 4 and 1 x 1 km resolution during February 2017.

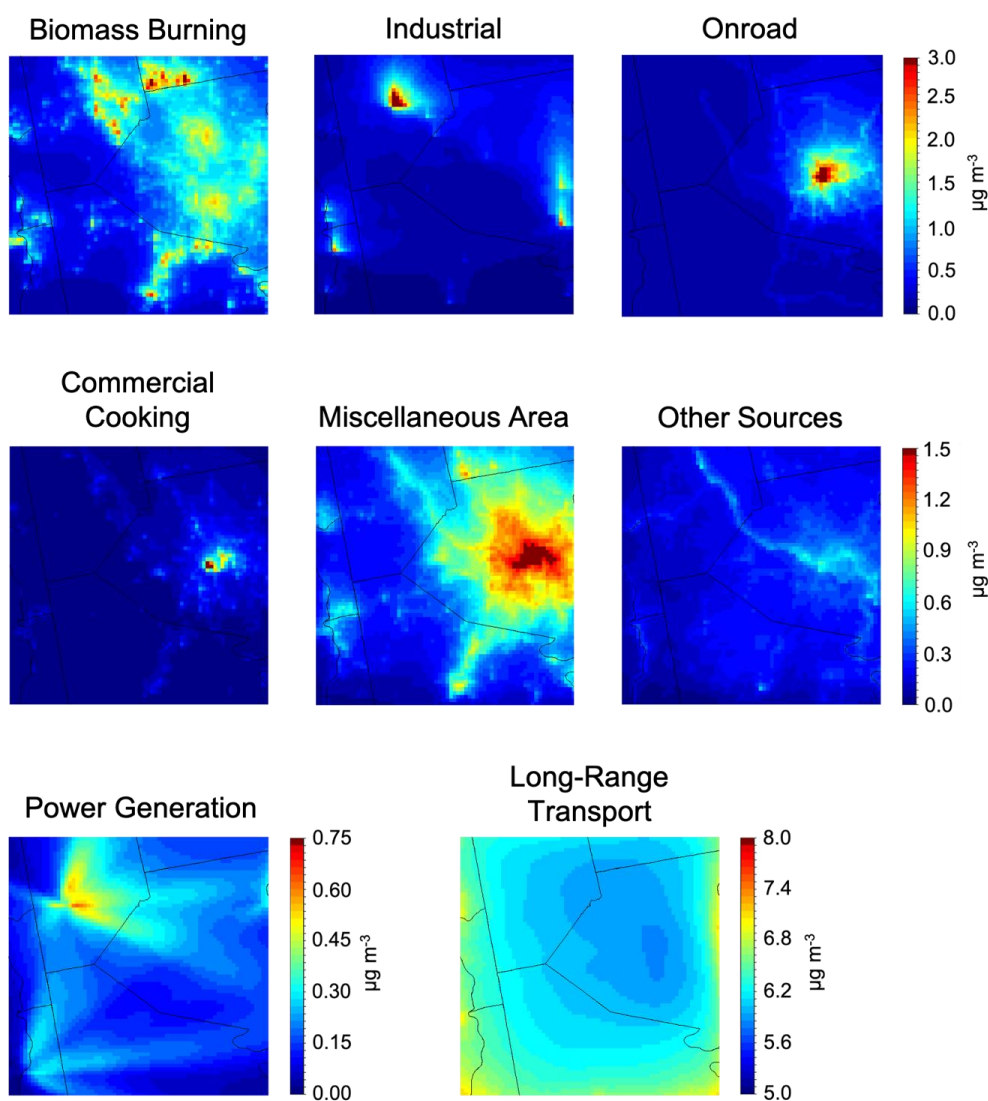
634 Different scales are used for the various maps.

635

636



637



638

639

640 **Figure 5.** Contribution of each source to total  $PM_{2.5}$  during February 2017. Different scales  
 641 are used for the various maps.

642

643

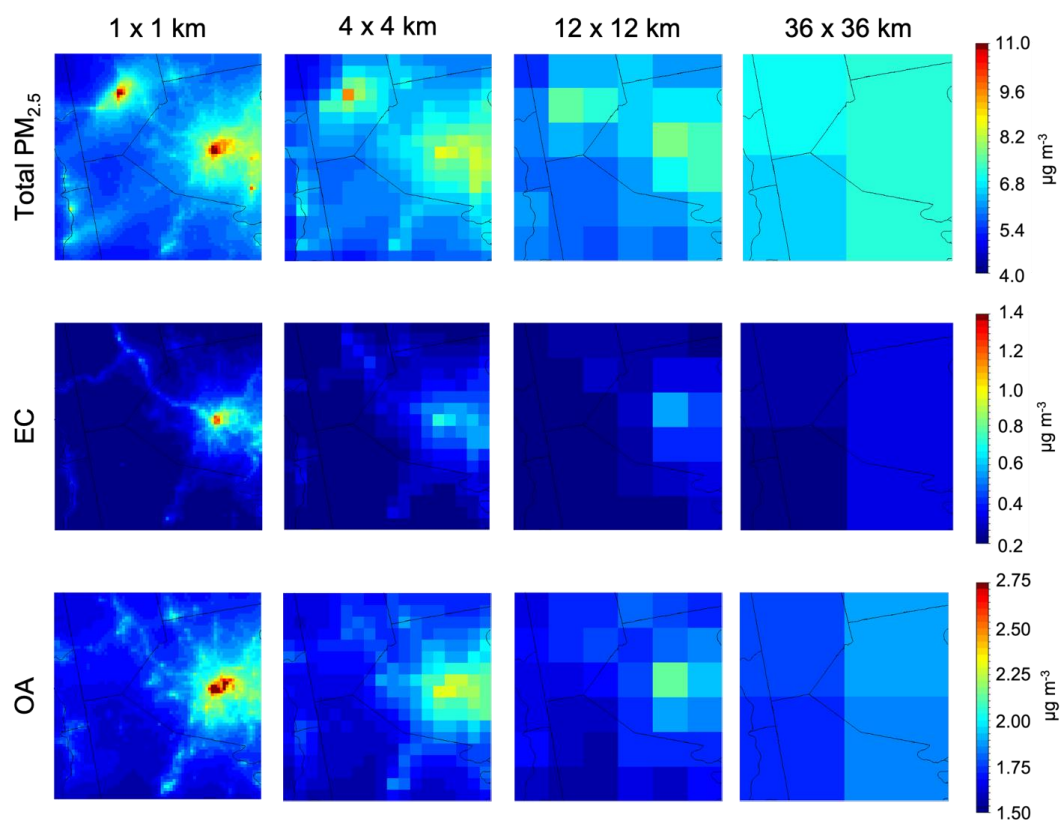
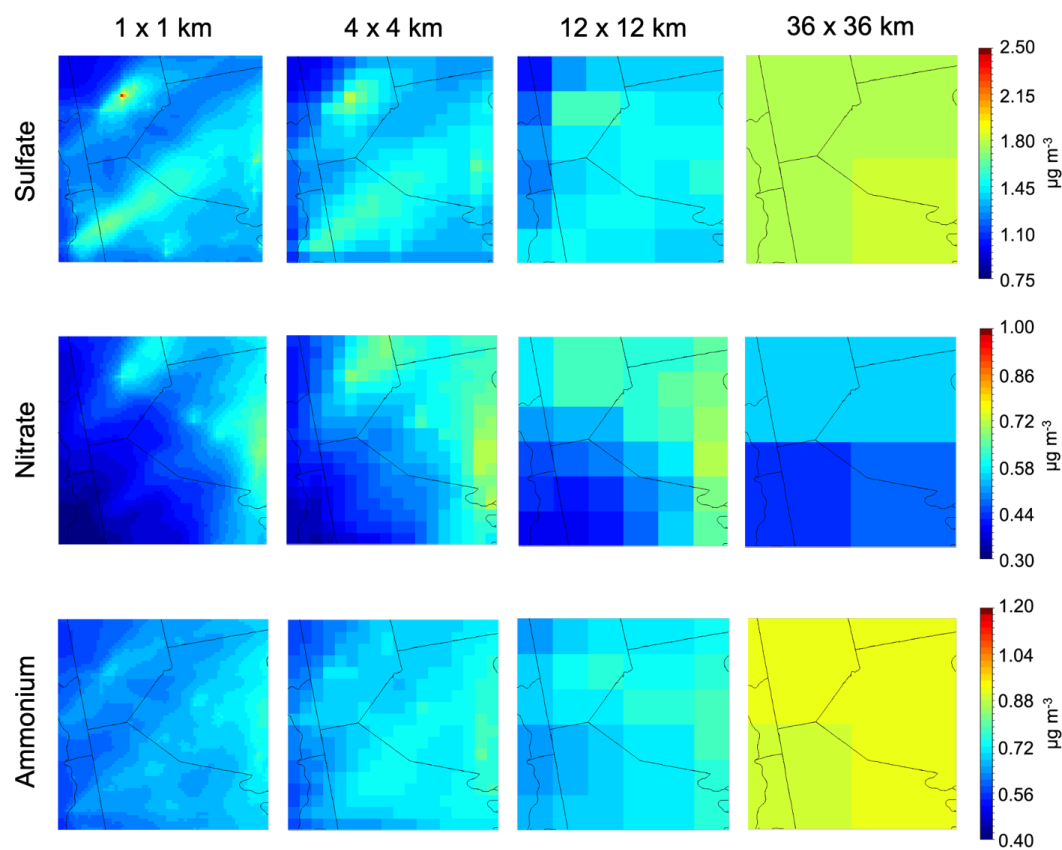


**Figure 6** Average predicted concentration at the ground level of total  $\text{PM}_{2.5}$ , EC and OA at a 36x36, 12x12, 4x4 and 1x1 km during July 2017. Different scales are used for the various maps.



650



651

652 **Figure 7** Average predicted concentration of PM<sub>2.5</sub> sulfate, nitrate, and ammonium at a  
 653 36x36, 12x 12, 4x4 and 1x1 km during July 2017. Different scales are used for the various  
 654 maps.

655

656

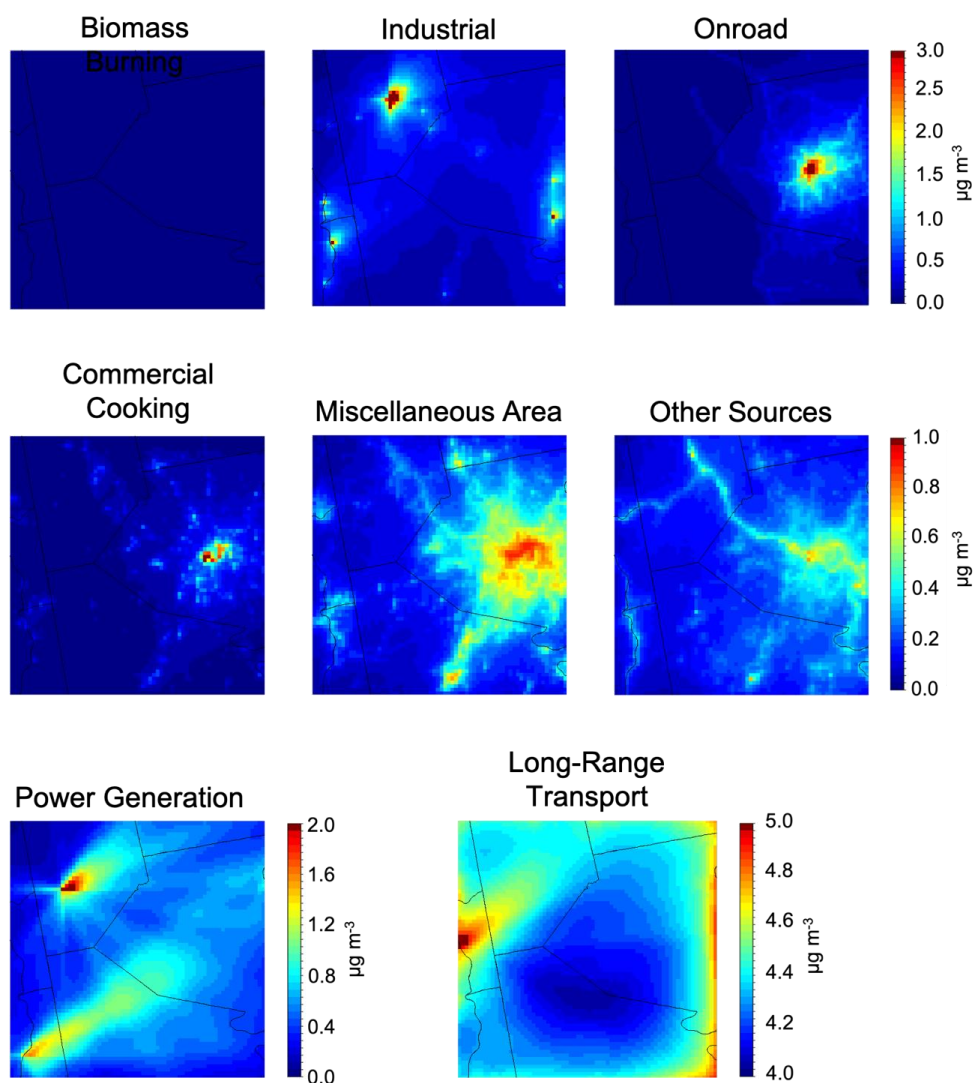


**Figure 8** Contribution of each source to total PM<sub>2.5</sub> during July 2017. Different scales are used for the various maps.

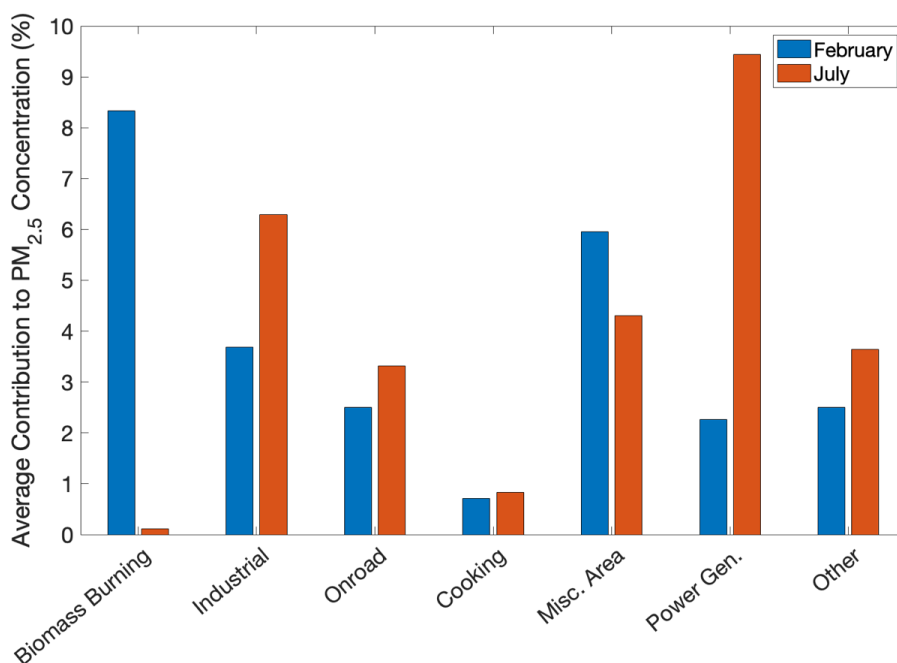
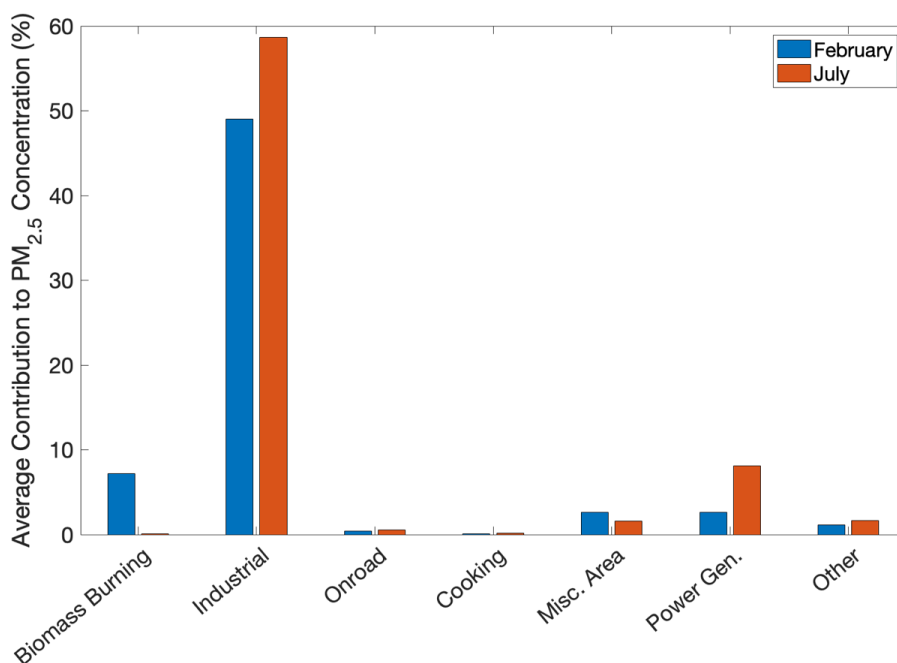


**Figure 9** Relative contributions of local sources to average predicted total  $PM_{2.5}$  concentrations in the Allegheny County simulation domain during February and July 2017.



667

668 **Figure 10** Relative contributions of local sources to average predicted PM<sub>2.5</sub> concentrations  
 669 at the location of highest average concentration (Butler County) during February and July  
 670 2017.

671



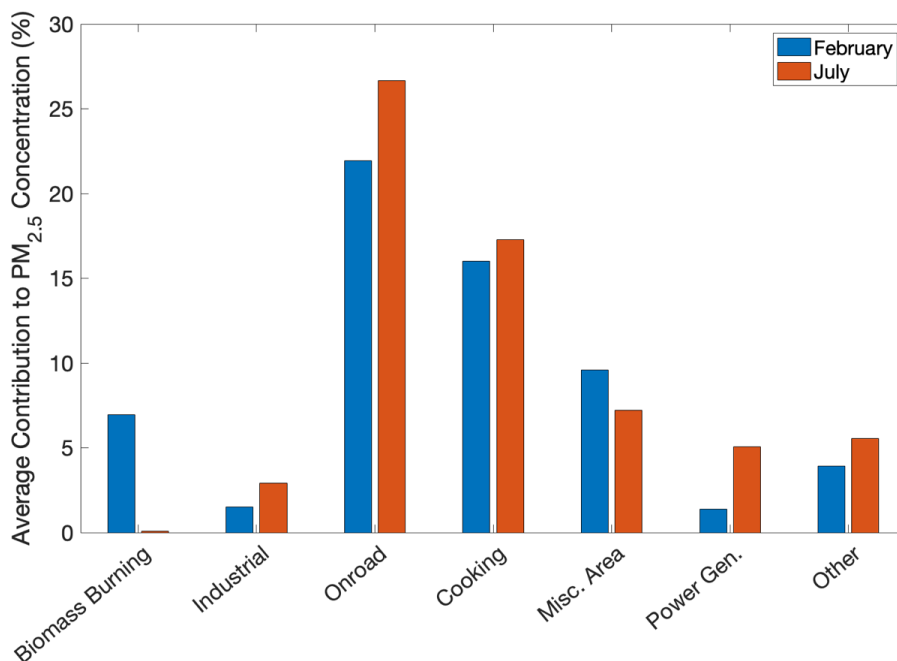
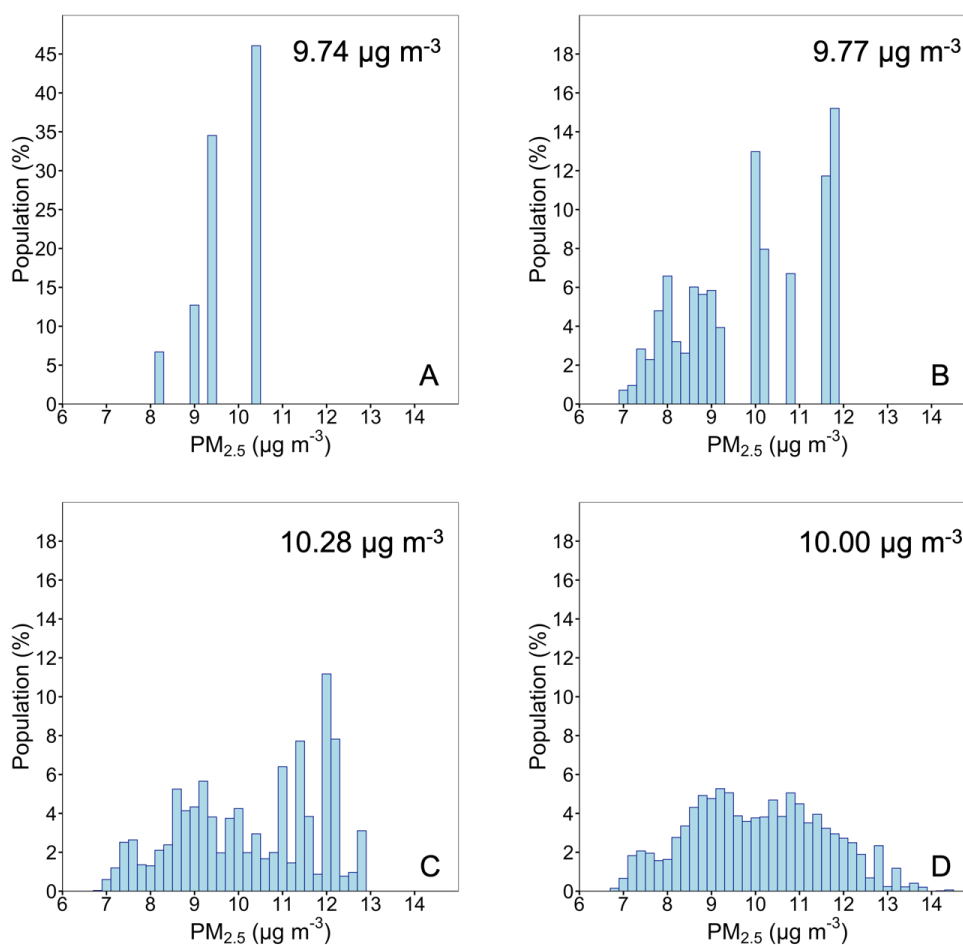


**Figure 11** Relative contributions of local sources to average predicted total  $PM_{2.5}$  concentrations in downtown Pittsburgh during February and July 2017.



676



677

678

679 **Figure 12** Population exposure histograms at (A) 36x36, (B) 12x 12, (C) 4x4 and (D) 1x1  
 680 km during February 2017. A different scale for population is used for the distribution at 36  
 681 x 36 km resolution. The average population weighted  $PM_{2.5}$  concentration for each  
 682 resolution is shown in the upper right corner of each window.

683

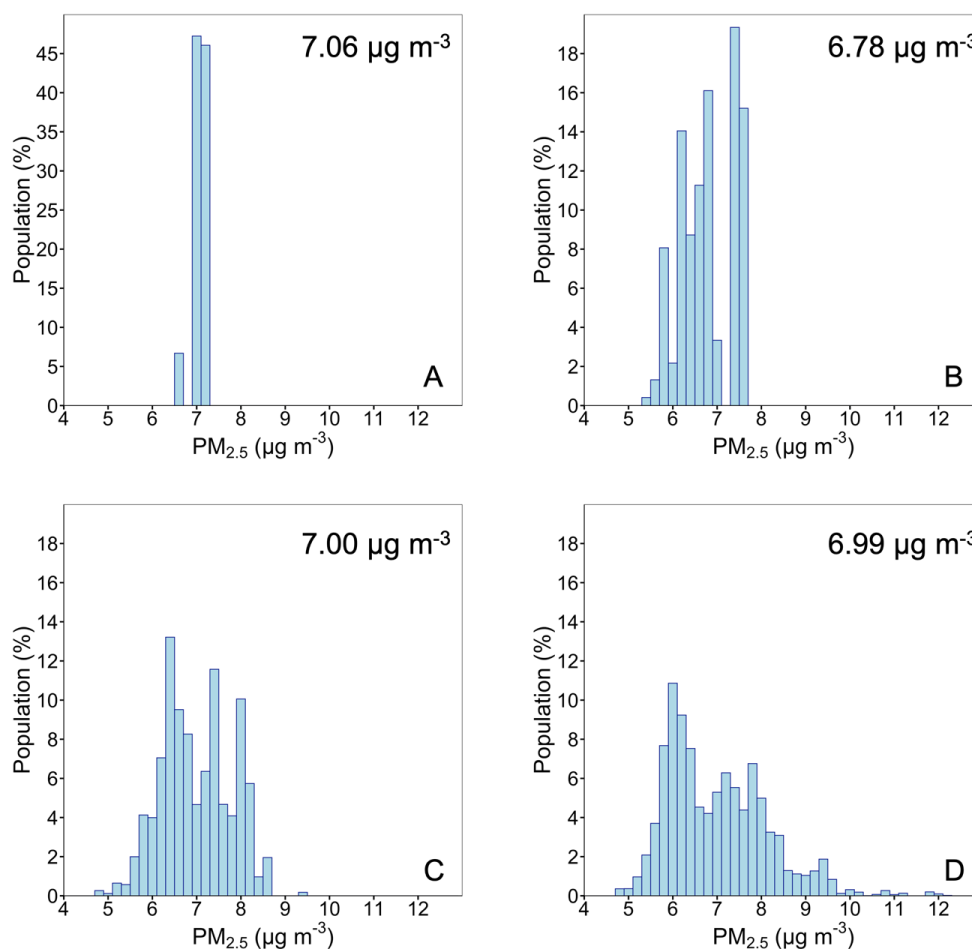
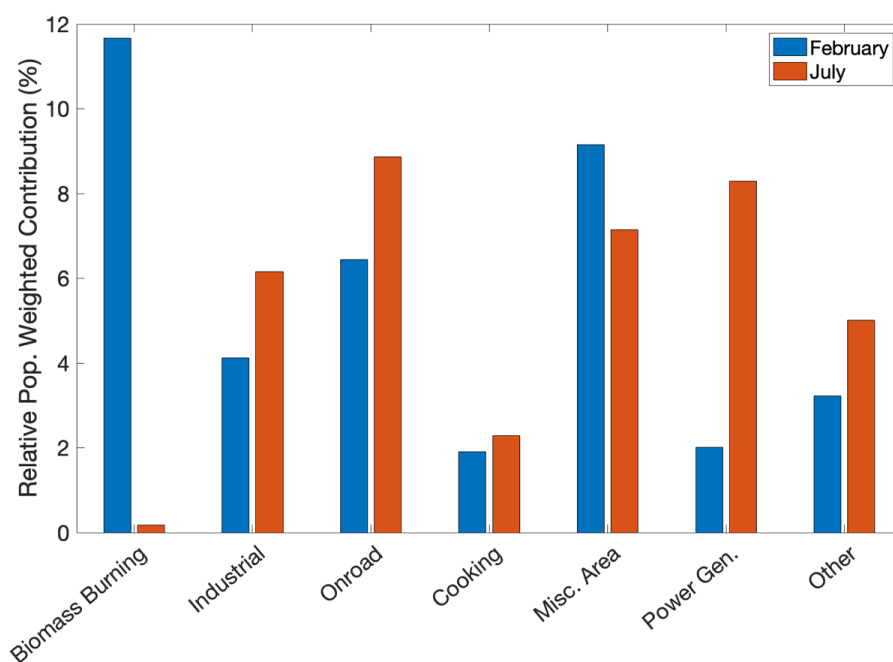


**Figure 13** Population exposure histograms at (A) 36x36, (B) 12x 12, (C) 4x4 and (D) 1x1 km during July 2017. A different scale for population is used for the distribution at 36 x 36 km resolution. The average population weighted  $PM_{2.5}$  concentration for each resolution is shown in the upper right corner of each window.



691

692



693

694 **Figure 14** Relative contributions from local sources to population weighted total  $PM_{2.5}$   
 695 concentration for February and July 2017.

696